New Journal of Glass and Ceramics, 2017, 7, 58-76
http://www.scirp.org/journal/njgc
ISSN Online: 2161-7562
ISSN Print: 2161-7554

Additive Effects of Rare-Earth Ions in Sodium Aluminoborate Glasses Using ^{23}Na and ^{27}Al Magic Angle Spinning Nuclear Magnetic Resonance

Shunichi Kaneko[1], Yomei Tokuda[2*], Hirokazu Masai[1]

[1]Institute for Chemical Research, Kyoto University, Uji City, Kyoto, Japan
[2]Faculty of Education, Shiga University, Hiratsu Otsu City, Shiga, Japan
Email: *tokuda@edu.shiga-u.ac.jp

How to cite this paper: Kaneko, S., Tokuda, Y. and Masai, H. (2017) Additive Effects of Rare-Earth Ions in Sodium Aluminoborate Glasses Using ^{23}Na and ^{27}Al Magic Angle Spinning Nuclear Magnetic Resonance. *New Journal of Glass and Ceramics*, **7**, 58-76.
https://doi.org/10.4236/njgc.2017.73006

Received: April 20, 2017
Accepted: July 4, 2017
Published: July 7, 2017

Abstract

We conducted structural analysis of xNa$_2$O-yY$_2$O$_3$-5B$_2$O$_3$-3Al$_2$O$_3$ and xNa$_2$O-yLa$_2$O$_3$-5B$_2$O$_3$-3Al$_2$O$_3$ glasses to elucidate the additive effects of rare-earth ions in these sodium aluminoborate glasses, and investigated the local environment surrounding Na$^+$ in them by using ^{23}Na and ^{27}Al magic angle spinning nuclear magnetic resonance (MAS NMR) spectroscopy. The amount of higher-coordinated Al species ($^{[5]}$Al and $^{[6]}$Al) gradually increased in response to an increase in the ratios of Y$_2$O$_3$ to Al$_2$O$_3$ and La$_2$O$_3$ to Al$_2$O$_3$ in each type of glass, respectively. Moreover, the difference in the cation field strength (CFS) between Y^{3+} and La^{3+} was observed to affect the generation of $^{[5]}$Al and $^{[6]}$Al, especially when the amount of these ions in the glasses increased. In addition to the above, the coordination number of Na$^+$ ions increased with an increase in the number of rare earth ions, confirmed by comparing results with NMR spectra of crystalline Na$_2$Al$_2$B$_2$O$_7$. The latter possibly occurred due to the oxygen concentration on Al$^{[5]}$ and Al$^{[6]}$. Finally, it was confirmed that the formation of $^{[5]}$Al and $^{[6]}$Al decreases molar volume in oxide glasses, which might be partially due to better atomic packing of $^{[5]}$Al and $^{[6]}$Al.

Keywords

NMR, Aluminoborate, Rare-Earth

1. Introduction

In the past decades, much attention has been paid to aluminate glasses, such as

aluminoborate, aluminosilicate, or aluminoborosilicate glass, because the addition of α-alumina to oxide glasses results in high chemical stability [1] and/or ideal mechanical properties [2]. In such oxide glasses, three kinds of Al coordination exist: 4-coordinated $^{[4]}$Al, 5-coordinated $^{[5]}$Al, and 6-coordinated $^{[6]}$Al, which can all be quantitatively measured by magic angle spinning nuclear magnetic resonance (MAS NMR) [3] [4]. Using structural analysis of aluminate glasses using MAS NMR, it has been clarified that their physical properties, such as fictive temperature, microhardness, elastic modulus, and refractive index, are closely related to their Al coordination [5] [6] [7] [8]. Therefore, it is important to control Al coordination in oxide glasses for adjustments of those physical properties.

In earlier reports, the relationship between the addition of network modifiers and generation of aluminum species has been reported. In particular, rare-earth ions (RE^{3+}) such as Sc^{3+}, Y^{3+}, or La^{3+} could produce higher-coordinated Al species ($^{[5]}$Al and $^{[6]}$Al) because they exhibit a sufficiently large cation field strength of CFS = z/R^2, where z is the ionic valence and R is the ionic radius [9] [10] [11] [12] [13]. Despite this, the glass-forming compositions of rare-earth-containing glasses were limited by high melting points of starting materials such as Y_2O_3 or Al_2O_3 [14] [15] [16]. Hence, control of $^{[5]}$Al and $^{[6]}$Al formation was still difficult, and one of the few ways to control Al speciation was by using different ions (e.g., the CFS of Mg^{2+} is lower than that of rare-earth ions, which suppressed the formation of $^{[5]}$Al and $^{[6]}$Al). Considering the development of functional glasses, it is important to investigate the relation between more complex compositions, Al coordination, and physical properties, because commercially used glass for optical or building applications contains several elements. Therefore, it would be interesting if, even in glasses that contain four or five elements, rare-earth ions can produce higher coordinated Al species that affect the physical properties of the glass.

We considered that the addition of Na^+ to aluminoborate glasses that contain several RE^{3+} species could expand the glass formation region and generate the intended amounts of $^{[5]}$Al and $^{[6]}$Al, proportional to the ratio of RE^{3+} to Al_2O_3. Although NMR analysis of various aluminoborate glasses has been performed (e.g., Na_2O-B_2O_3-Al_2O_3, Y_2O_3-B_2O_3-Al_2O_3, or La_2O_3-B_2O_3-Al_2O_3) [17]-[24], most of these analyses have been done with mono-network modifiers. Herein, we structurally analyzed yttrium sodium aluminoborate and lanthanum sodium aluminoborate glasses in order to observe the relationship between the addition of RE^{3+} and the formation of $^{[5]}$Al and $^{[6]}$Al. Simultaneously, we investigated the local structure of Na^+ in order to understand its role in these glasses. Finally, we measured the molar volumes in these glasses in order to understand the direct relationship between the formed amounts of $^{[5]}$Al and $^{[6]}$Al and the physical properties of the glasses. As a result of the above experiment, the structural roles of RE^{3+}, Na^+ and Al^{3+} in quaternary aluminoborate glass have been clarified.

2. Experimental

2.1. Synthesis

2.1.1. Preparation of Sample Glasses

All glass samples were prepared using a melting method from chemically pure Na_2CO_3, Y_2O_3, La_2O_3, $B(OH)_3$, and Al_2O_3 as starting materials. Stoichiometric powders were mixed using agate mortar and melted in a platinum crucible at 1550˚C - 1600˚C for 30 min. Subsequently, melts were quenched by a metal plate that was pre-heated to 300˚C in order to prevent them from cracking. The glasses thus obtained had compositions of xNa$_2$O-yY$_2$O$_3$-5B$_2$O$_3$-3Al$_2$O$_3$ and xNa$_2$O-yLa$_2$O$_3$-5B$_2$O$_3$-3Al$_2$O$_3$, with (x, y) combinations of (6, 0), (4.8, 0.4), (3.96, 0.66), (3, 1), (1.98, 1.32), (1.2, 1.6) and (0, 2). Considering Al_2O_3 and B_2O_3 as network modifiers, the total cation valence was set to be +12 in all compositions in order to keep ratio of cation valence to network modifier unchanged. Glass transition temperatures (T_g) were measured by differential thermal analysis (DTA, Thermo Plus 8120, Rigaku, Tokyo, Japan) and are shown in Table 1 and Table 2. Although we tried to analyze the composition of the synthesized glass with inductively-coupled plasma atomic emission spectrometry and X-ray Fluorescence, the detection accuracy of these instruments for boron was too low to measure the composition of all samples with high accuracy. However, T_g of our glasses showed the additivity. Hence, the compositions of all glasses are given as batch compositions in this report (Table 1 and Table 2).

Table 1. The composition and glass transition temperature of xNa$_2$O-yY$_2$O$_3$-5B$_2$O$_3$-3Al$_2$O$_3$ glasses.

(x, y)	Na_2O (mol%)	Y_2O_3 (mol%)	B_2O_3 (mol%)	Al_2O_3 (mol%)	Y_2O_3/Al_2O_3	T_g^a (˚C)
(6, 0)	42.9	0.0	35.7	21.4	0.0	392
(4.8, 0.4)	36.4	3.0	37.9	22.7	0.13	449
(3.96, 0.66)	31.4	5.2	39.6	23.8	0.22	472
(3, 1)	25.0	8.3	41.7	25.0	0.33	512
(1.98, 1.32)	17.5	11.7	44.2	26.5	0.44	560
(1.2, 1.6)	11.1	14.8	46.3	27.8	0.53	630
(0, 2)	0.0	20.0	50.0	30.0	0.67	727

[a]uncertainty in T_g is ± 1˚C.

Table 2. The composition and glass transition temperature of xNa$_2$O-yLa$_2$O$_3$-5B$_2$O$_3$-3Al$_2$O$_3$ glasses.

(x, y)	Na_2O (mol%)	La_2O_3 (mol%)	B_2O_3 (mol%)	Al_2O_3 (mol%)	La_2O_3/Al_2O_3	T_g^a (˚C)
(6, 0)	42.9	0.0	35.7	21.4	0.0	392
(4.8, 0.4)	36.4	3.0	37.9	22.7	0.13	460
(3.96, 0.66)	31.4	5.2	39.6	23.8	0.22	480
(3, 1)	25.0	8.3	41.7	25.0	0.33	499
(1.98, 1.32)	17.5	11.7	44.2	26.5	0.44	543
(1.2, 1.6)	11.1	14.8	46.3	27.8	0.53	584
(0, 2)	0.0	20.0	50.0	30.0	0.67	671

[a]uncertainty in T_g is ±1˚C.

2.1.2. Preparation of Crystalline $Na_2Al_2B_2O_7$

Crystalline $Na_2Al_2B_2O_7$ was synthesized to confirm the relationship between the local structure of Na^+ at different sites in the crystal and the chemical shifts of ^{23}Na NMR spectra. The crystal sample was prepared using a previously-reported solid state reaction [25]. Briefly, a stoichiometric mixture of $NaHCO_3$, $B(OH)_3$, and Al_2O_3 was crushed thoroughly in an agate mortar, calcined at 400˚C for 10 h, and finally heated at 950˚C for 48 h.

2.2. Measurements

2.2.1. Characterization of Crystal Samples

Synthesized samples were analyzed using X-ray diffraction (XRD, Rigaku, RINT-2100, Tokyo, Japan). In addition, the XRD patterns were also simulated with known crystallographic information [25] using the Mercury software.

2.2.2. NMR Spectroscopy

Solid-state ^{23}Na and ^{27}Al MAS NMR spectra of all crystal and glass samples were acquired on an AVANCE III spectrometer (Bruker, Billerica, MA) using a commercial probe (4 mm). The rotation speed was set to 15 kHz with an accuracy of ± 1 Hz. Under an external field of 18.8 T, the resonance frequencies for ^{23}Na and ^{27}Al were near 212 and 208 MHz, respectively. Each measurement was conducted using single-pulse sequence. 90˚ pulses were set to 7 μs for ^{23}Na. The complete relaxation was confirmed in this condition. In addition, in the case of ^{27}Al, 0.63 μs pulse which is corresponding to a radiofrequency tip angle 24˚ was applied to ensure quantitative measurement of Al spices. Spectra were obtained with a cycle time of 2 s for both ^{23}Na and ^{27}Al. Aqueous solutions of 1 M NaCl and 1 M $Al(NO_3)_3$ were used as references, with their chemical shifts set to 0 ppm. The ^{23}Na spectra were normalized, so that the total area in each spectrum is proportional to the alkali content. This way, the areas of the spectra can be compared with each other.

2.2.3. Density

The Archimedes method was used for density measurements of synthesized glasses and to calculate molar volumes.

3. Results

3.1. ^{27}Al MAS NMR

The ^{27}Al MAS NMR spectra of yttrium sodium aluminoborate glasses and lanthanum sodium aluminoborate glasses are shown in **Figure 1** and **Figure 2**, respectively. The intensity of the $^{[4]}Al$ peaks in these spectra were set to be same. The peak of $^{[4]}Al$ gradually shifted upfield in response to the increase of Y^{3+}. In order to fit the experimental spectra, gaussian functions were used. We considered that the magnetic field of MAS NMR was strong (18.8 T) enough to neglect quadrupolar shift and broadening effects. The error of the total fitting curve for $^{[4]}Al$, $^{[5]}Al$ and $^{[6]}Al$ was calculated to be 1% - 6% in all glasses.

As a result of this, each of the errors for $^{[4]}Al$, $^{[5]}Al$ and $^{[6]}Al$ is expected to be

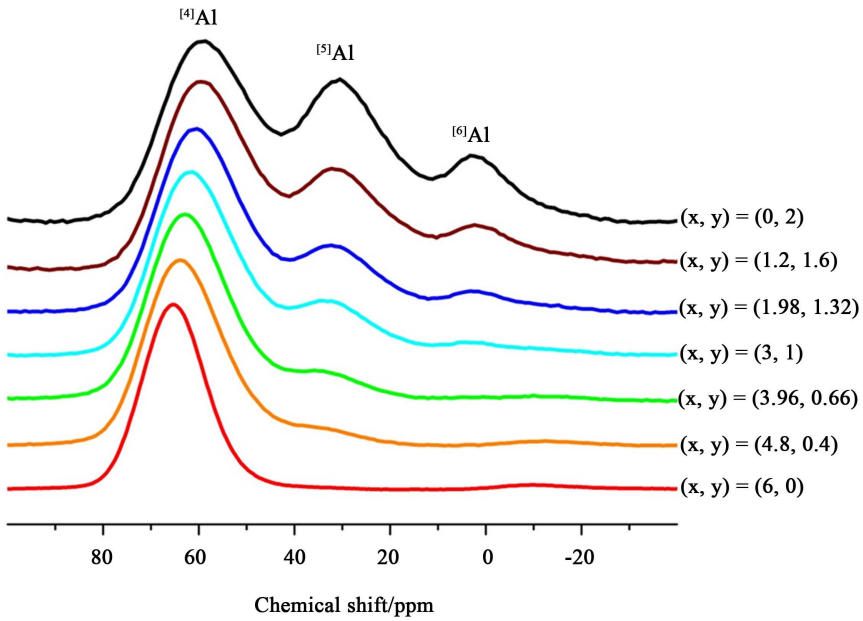

Figure 1. ^{27}Al magic angle spinning nuclear magnetic resonance (MAS NMR) spectra of xNa$_2$O-yY$_2$O$_3$-5B$_2$O$_3$-3Al$_2$O$_3$ glasses.

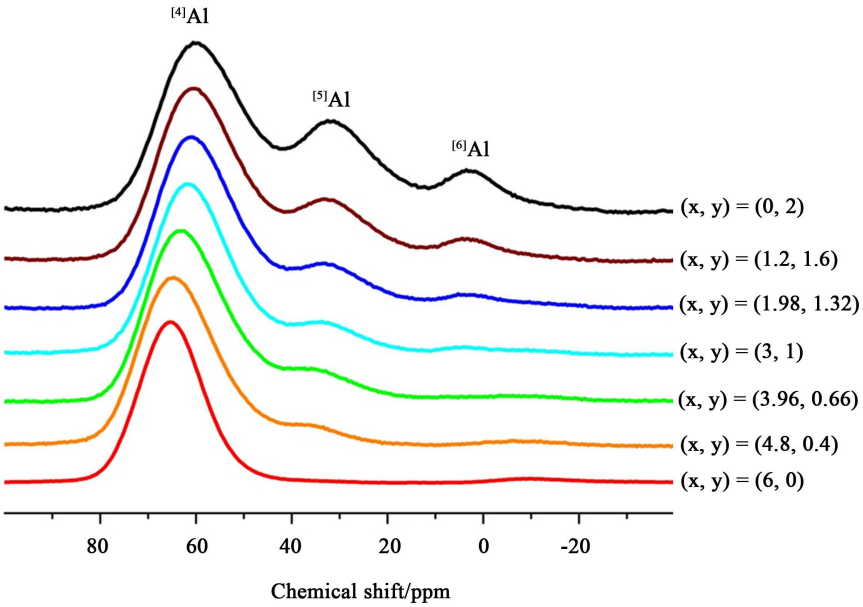

Figure 2. ^{27}Al MAS NMR spectra of xNa$_2$O-yLa$_2$O$_3$-5B$_2$O$_3$-3Al$_2$O$_3$ glasses.

less than 1% - 6%. Deconvolution of these spectra into the $^{[4]}$Al (around 60 ppm), $^{[5]}$Al (around 30 ppm), and $^{[6]}$Al (around 0 ppm) peaks indicated that the fraction of each Al species changed substantially (Figures 3-15). As the proportion of Y$_2$O$_3$ in the glass increased, the fraction of $^{[4]}$Al decreased from 99 to 48%, that of $^{[5]}$Al increased from 1 to 36%, and that of $^{[6]}$Al increased from 0 to 16% (Figure 16 and Table 3). For lanthanum sodium aluminoborate glass, likewise, the fraction of $^{[4]}$Al decreased from 99 to 57%, that of $^{[5]}$Al increased from 1 to 30%, and that of $^{[6]}$Al increased from 0 to 13% (Figure 17 and Table 4).

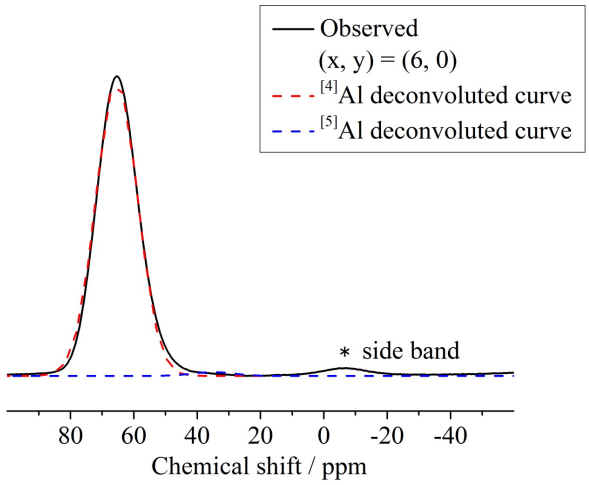

Figure 3. Peak deconvolution of ^{27}Al MAS NMR spectrum of $6Na_2O$-$5B_2O_3$-$3Al_2O_3$ glass.

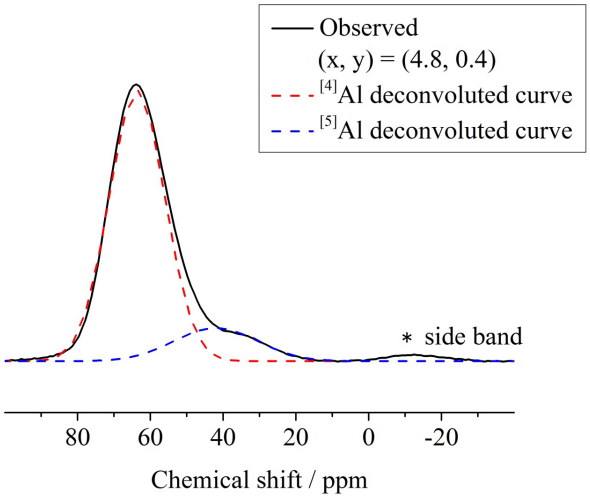

Figure 4. Peak deconvolution of ^{27}Al MAS NMR spectrum of $4.8Na_2O$-$0.4Y_2O_3$-$5B_2O_3$-$3Al_2O_3$ glass.

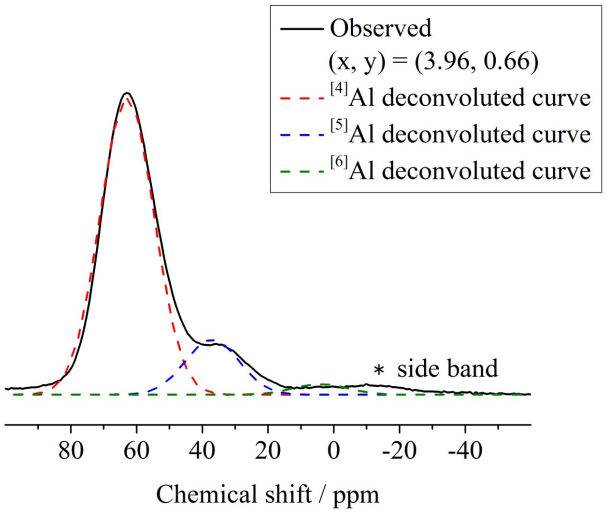

Figure 5. Peak deconvolution of ^{27}Al MAS NMR spectrum of $3.96Na_2O$-$0.66Y_2O_3$-$5B_2O_3$-$3Al_2O_3$ glass.

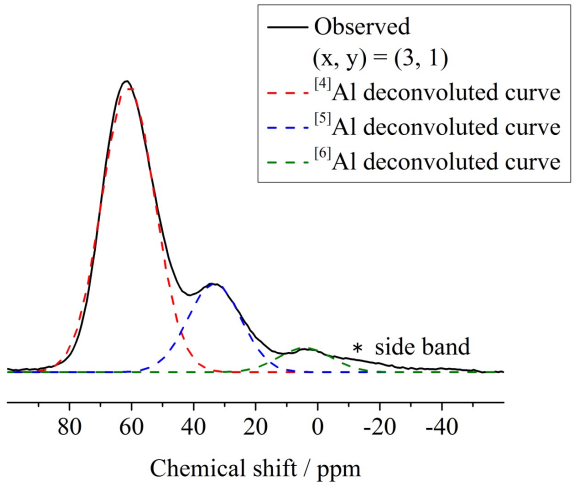

Figure 6. Peak deconvolution of ^{27}Al MAS NMR spectrum of $3Na_2O$-Y_2O_3-$5B_2O_3$-$3Al_2O_3$ glass.

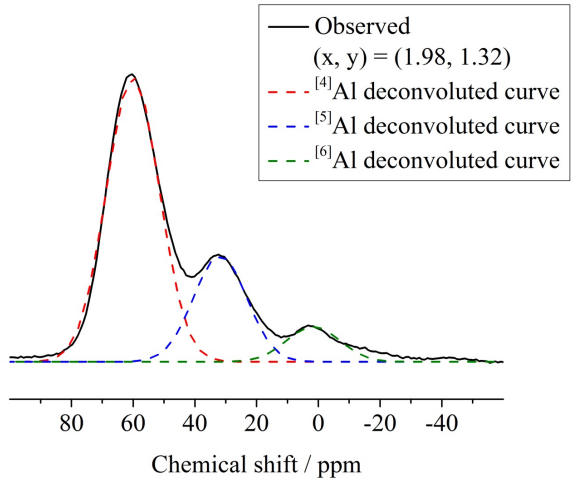

Figure 7. Peak deconvolution of ^{27}Al MAS NMR spectrum of $1.98Na_2O$-$1.32Y_2O_3$-$5B_2O_3$-$3Al_2O_3$ glass.

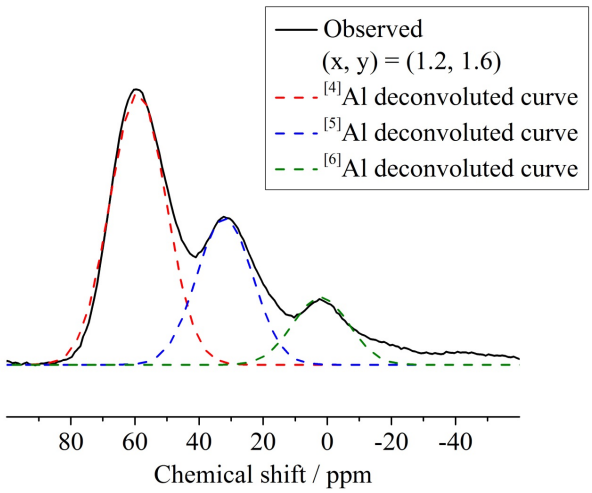

Figure 8. Peak deconvolution of ^{27}Al MAS NMR spectrum of $1.2Na_2O$-$1.6\ Y_2O_3$-$5B_2O_3$-$3Al_2O_3$ glass.

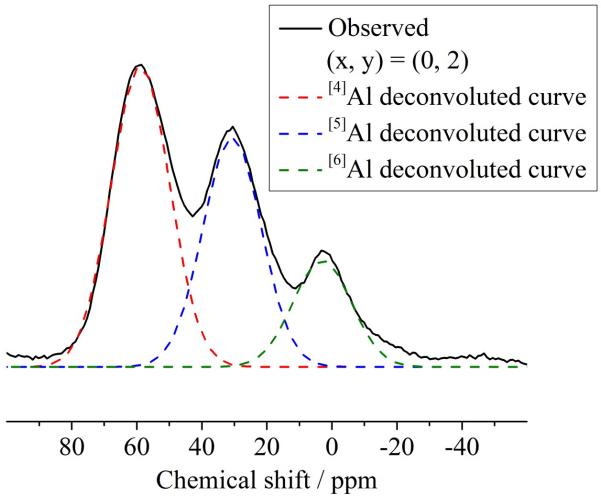

Figure 9. Peak deconvolution of ^{27}Al MAS NMR spectrum of $2Y_2O_3$-$5B_2O_3$-$3Al_2O_3$ glass.

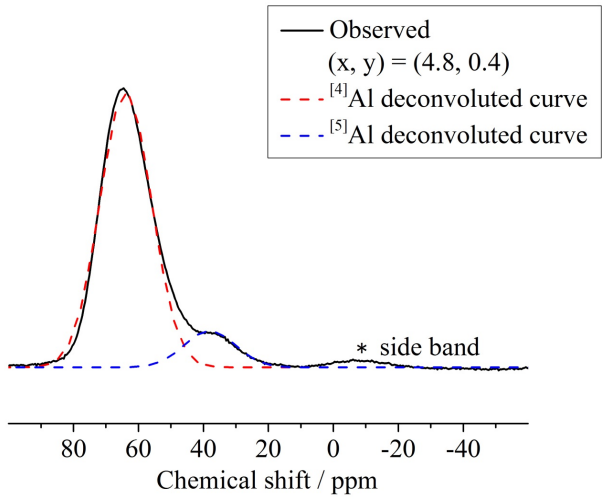

Figure 10. Peak deconvolution of ^{27}Al MAS NMR spectrum of $4.8Na_2O$-$0.4La_2O_3$-$5B_2O_3$-$3Al_2O_3$ glass.

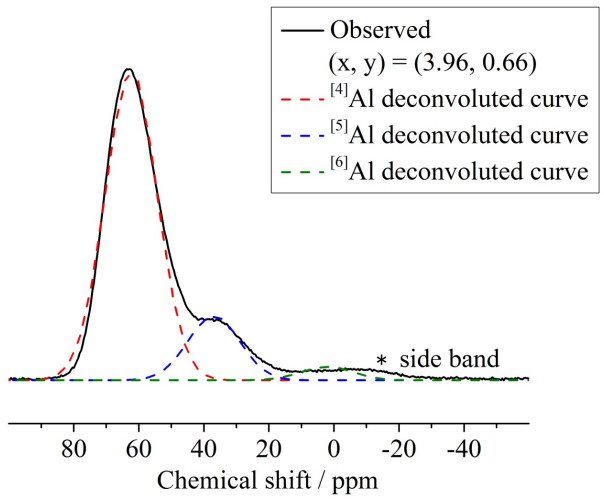

Figure 11. Peak deconvolution of ^{27}Al MAS NMR spectrum of $3.96Na_2O$-$0.66La_2O_3$-$5B_2O_3$-$3Al_2O_3$ glass.

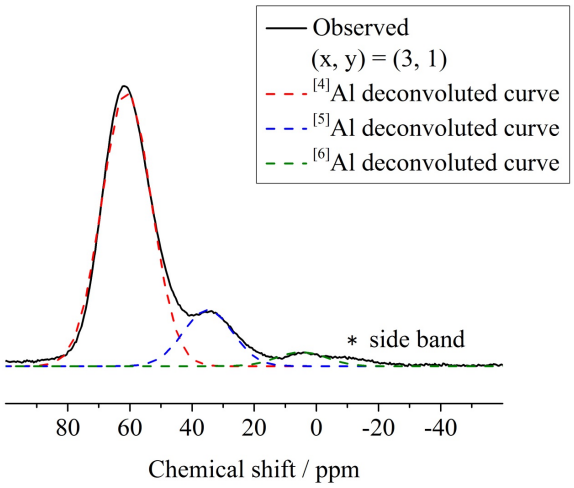

Figure 12. Peak deconvolution of ^{27}Al MAS NMR spectrum of $3Na_2O$-La_2O_3-$5B_2O_3$-$3Al_2O_3$ glass.

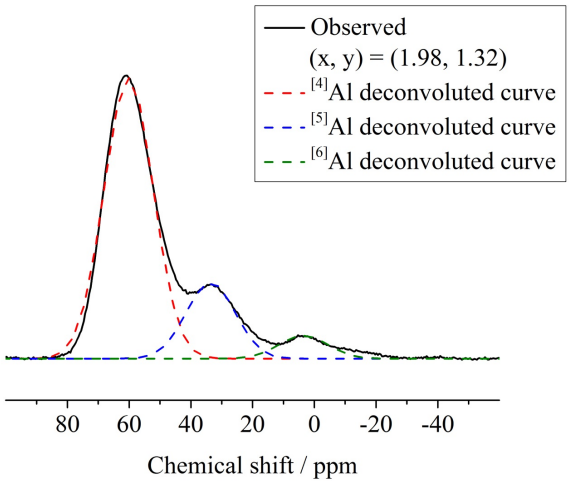

Figure 13. Peak deconvolution of ^{27}Al MAS NMR spectrum of $1.98Na_2O$-$1.32La_2O_3$-$5B_2O_3$-$3Al_2O_3$ glass.

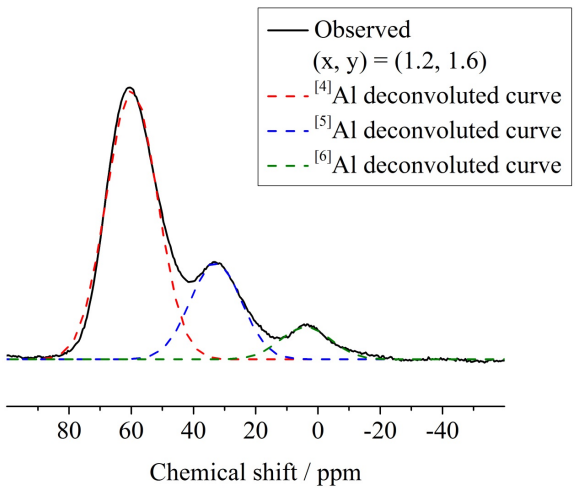

Figure 14. Peak deconvolution of ^{27}Al MAS NMR spectrum of $1.2Na_2O$-$1.6\ La_2O_3$-$5B_2O_3$-$3Al_2O_3$ glass.

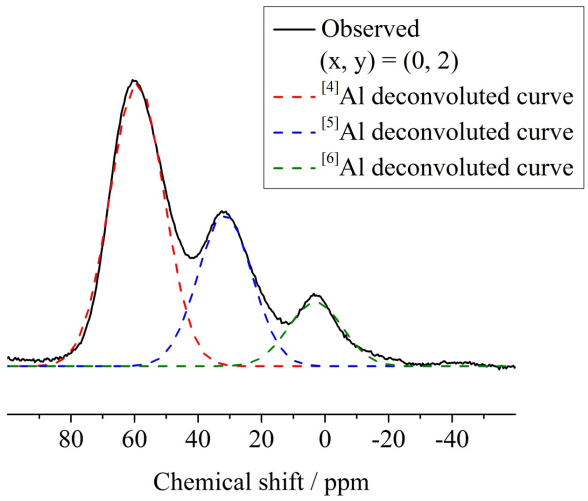

Figure 15. Peak deconvolution of ^{27}Al MAS NMR spectrum of $2La_2O_3$-$5B_2O_3$-$3Al_2O_3$ glass.

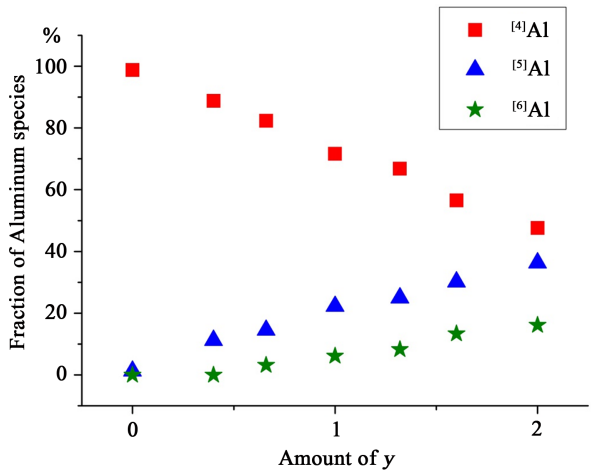

Figure 16. $^{[4]}$Al, $^{[5]}$Al, and $^{[6]}$Al as fractions of total Al in xNa$_2$O-yY$_2$O$_3$-$5B_2O_3$-$3Al_2O_3$ glasses.

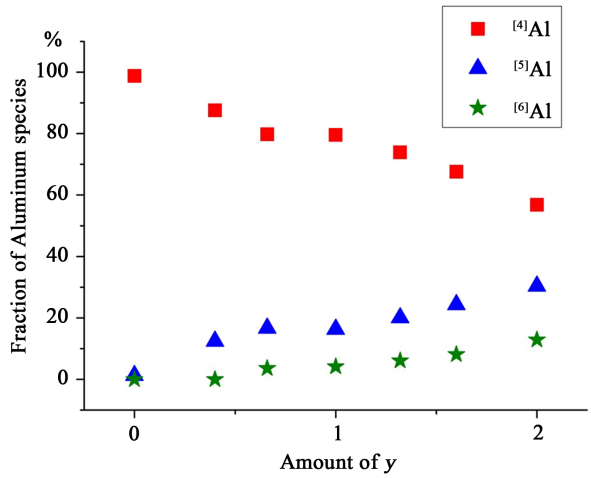

Figure 17. $^{[4]}$Al, $^{[5]}$Al, and $^{[6]}$Al as fractions of total Al in xNa$_2$O-yLa$_2$O$_3$-$5B_2O_3$-$3Al_2O_3$ glasses.

Table 3. Al speciation of xNa$_2$O-yY$_2$O$_3$-5B$_2$O$_3$-3Al$_2$O$_3$ glasses.

(x, y)	$^{[4]}$Al (%)	$^{[5]}$Al (%)	$^{[6]}$Al (%)	$^{[5]}$Al + $^{[6]}$Al (%)
(6, 0)	99	1	~0	1
(4.8, 0.4)	89	11	~0	11
(3.96, 0.66)	82	15	3	18
(3, 1)	72	22	6	28
(1.98, 1.32)	67	25	8	33
(1.2, 1.6)	57	30	13	43
(0, 2)	48	36	16	52

[a]uncertainty in the sum of $^{[4]}$Al + $^{[5]}$Al + $^{[6]}$Al is 1% - 5%.

Table 4. Al speciation of xNa$_2$O-yLa$_2$O$_3$-5B$_2$O$_3$-3Al$_2$O$_3$ glasses.

(x, y)	$^{[4]}$Al (%)	$^{[5]}$Al (%)	$^{[6]}$Al (%)	$^{[5]}$Al + $^{[6]}$Al (%)
(6, 0)	99	1	~0	1
(4.8, 0.4)	88	12	~0	12
(3.96, 0.66)	80	16	4	20
(3, 1)	79	17	4	21
(1.98, 1.32)	74	20	6	26
(1.2, 1.6)	68	24	8	32
(0, 2)	57	30	13	43

[a]uncertainty in the sum of $^{[4]}$Al + $^{[5]}$Al + $^{[6]}$Al is 1% - 6%.

3.2. XRD Pattern and ^{23}Na MAS NMR Spectrum of Crystalline $Na_2Al_2B_2O_7$

The XRD pattern of synthesized crystalline $Na_2Al_2B_2O_7$ and its pattern simulated by Mercury [25] are shown in **Figure 18**, while the ^{23}Na NMR spectrum of crystalline $Na_2Al_2B_2O_7$ is shown in **Figure 19**. Considering the 1:1 ratio of two sodium ion sites in crystalline $Na_2Al_2B_2O_7$, the peak area ratio should be 1. Nonetheless, there is a different crystal peak present in the lower field. However, according to a previous detailed study [26], the peak at the lower chemical shift can also be assigned to the Na^+ (2) site that is 9-coordinated with oxygen in the vicinity of Al, and the peak at the higher chemical shift can be assigned to the Na^+ (1) site that is 6-coordinated with oxygen in the vicinity of B (**Figure 19**).

3.3. ^{23}Na MAS NMR

The ^{23}Na MAS NMR spectra of yttrium sodium aluminoborate glasses and lanthanum sodium aluminoborate glasses are shown in **Figure 20** and **Figure 21**, respectively. The peak of the ^{23}Na spectra of Y^{3+}-containing glasses gradually shifted upfield in response to an increase of Y^{3+}. The peak shifted from −2.3 ppm at (x, y) = (6, 0) to −9.5 ppm at (x, y) = (1.2, 1.6). In the case of La^{3+}-containing glasses, a similar upfield spectral shift was observed. The peak shifted from ppm -2.3 ppm at (x, y) = (6, 0) to −10.0 ppm at (x, y) = (1.2, 1.6). Although there was

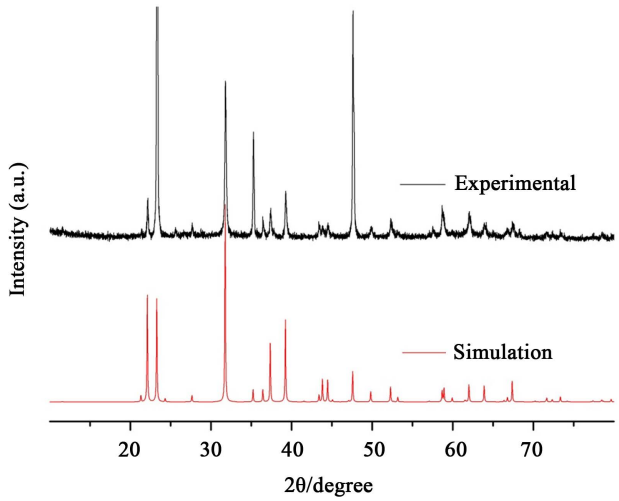

Figure 18. X-ray diffraction (XRD) pattern of crystalline $Na_2Al_2B_2O_7$. The XRD pattern of standard crystalline $Na_2Al_2B_2O_7$ obtained from simulation using Mercury software is also provided as reference.

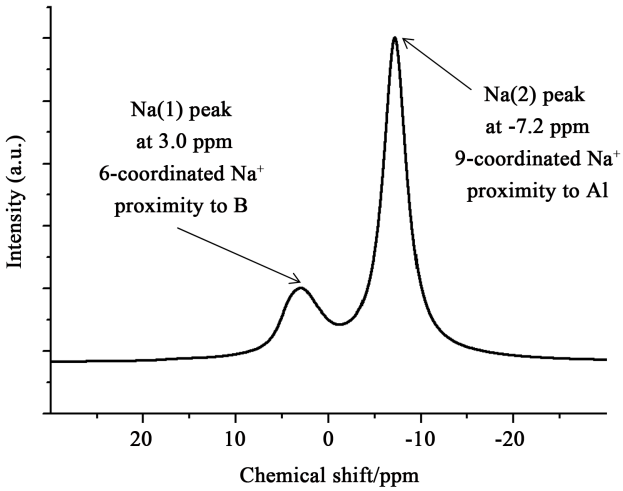

Figure 19. ^{23}Na MAS NMR spectra of crystalline $Na_2Al_2B_2O_7$.

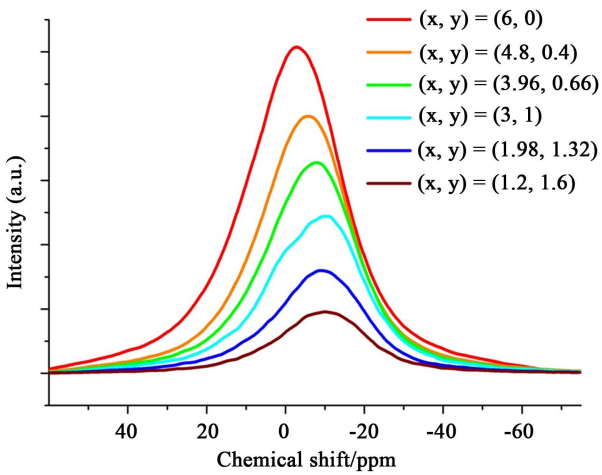

Figure 20. ^{23}Na MAS NMR spectra of xNa_2O-yY_2O_3-$5B_2O_3$-$3Al_2O_3$ glasses.

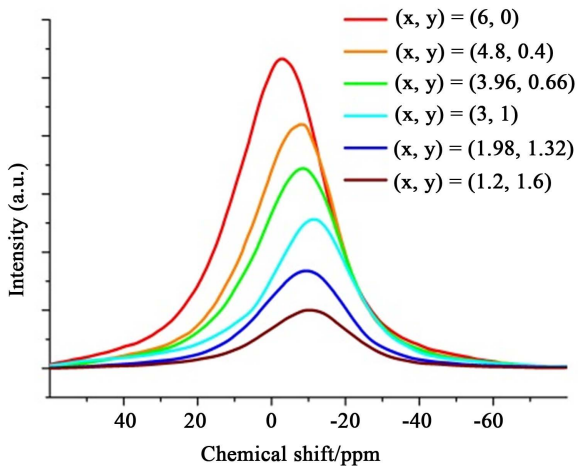

Figure 21. ^{23}Na MAS NMR spectra of xNa$_2$O-yLa$_2$O$_3$-5B$_2$O$_3$-3Al$_2$O$_3$ glasses.

a deviation when the composition was (x, y) = (3.1) (chemical shift at −11 ppm), the lower-magnetic field component clearly decreased in response to an increase in La^{3+}.

3.4. Molar Volume

The molar volumes of yttrium sodium aluminoborate and lanthanum sodium aluminoborate glasses are shown in **Figure 22**. As the RE^{3+} to Al_2O_3 ratio increased, the molar volume of the glasses steadily decreased.

4. Discussion

The ^{27}Al MAS NMR spectra clearly indicated that the fractions of $^{[5]}$Al and $^{[6]}$Al increased in response to an increase in the ratio of Y_2O_3 to Al_2O_3 (**Figure 1** and **Figure 16**). This result strongly suggests that Y^{3+} can produce higher-coordinated Al species despite the presence of Na^+. It was thus considered that the CFS of Y^{3+} is sufficiently larger than that of Na^+ to result in formation of $^{[5]}$Al and $^{[6]}$Al.

The relative amounts of $^{[5]}$Al and $^{[6]}$Al in Y^{3+}-containing glasses were larger than those in La^{3+}-containing glasses when the ratio of La_2O_3 to Al_2O_3 increased (**Figure 2** and **Figure 17**). It therefore seems that the difference in CFS between Y^{3+} and La^{3+} affected the formation of $^{[5]}$Al and $^{[6]}$Al. In previous studies [9] [10] [11] [12] [13], a greater CFS value resulted in a greater fraction of higher-coordinated Al in oxide glasses that contain RE^{3+} such as yttrium aluminosilicate or aluminoborate. As such, the above results further clarify that rare-earth ions with a large CFS can result in $^{[5]}$Al and $^{[6]}$Al even with co-existing Na^+. It was considered that most of RE^{3+} produced higher coordinated Al regardless of its composition because the combination of large CFS cation and higher coordinated Al could be energetically preferable [13].

Boron coordination is also important for elucidation of the local structure in this glass. Although we have measured ^{11}B MAS NMR spectra, it was difficult to complete peak deconvolution because the broad background components derived

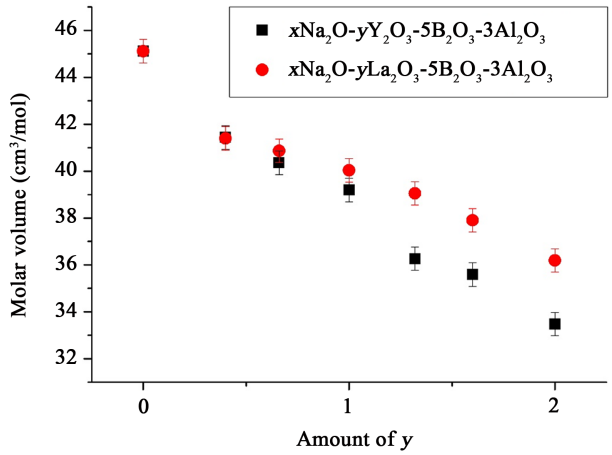

Figure 22. Molar volume of xNa$_2$O-yY$_2$O$_3$-5B$_2$O$_3$-3Al$_2$O$_3$ (■) and xNa$_2$O-yLa$_2$O$_3$-5B$_2$O$_3$-3Al$_2$O$_3$ glasses (●).

from instruments overlapped the corresponding spectrum of glass. Thus, we estimate the fraction of four-coordinated boron ($^{[4]}$B) in this glass system from the literatures. According to the earlier reports [24], 2Y$_2$O$_3$-5B$_2$O$_3$-3Al$_2$O$_3$ glass similar composition to our glass contains 12% of $^{[4]}$B. In the case of 2.5La$_2$O$_3$-5B$_2$O$_3$-2.5Al$_2$O$_3$, the amount of $^{[4]}$B is about 11% [15]. 4Na$_2$O-3B$_2$O$_3$-3Al$_2$O$_3$ and 5Na$_2$O-3.5B$_2$O$_3$-1.5Al$_2$O$_3$ glass were reported to contain 8.3% and 14.6% of $^{[4]}$B, respectively [27]. In addition, according to Chakraborty and Day [28], it was suggested that Al/B ratio is important for the nature of $^{[3]}$B/$^{[4]}$B ratio because $^{[4]}$B decreases with being replaced by larger $^{[4]}$Al sites. In this glass system, Al/B ratio is fixed at 0.6. Therefore, considering the above data and suggestion, it is assumed that amount of $^{[4]}$B did not greatly changed in respect to the composition in all glass system. The amount of $^{[4]}$B in the synthesized glass can be estimated as about 10% ± 5%.

The lower-field component of the ^{23}Na spectra of yttrium sodium aluminoborate glasses steadily decreased with respect to the increase in Y^{3+} (**Figure 20**). According to the ^{23}Na spectra of crystalline Na$_2$Al$_2$B$_2$O$_7$ (**Figure 19**), the peak attributed to 9-coordinated Na^+ (2) near Al is located upfield from that attributed to 6-coordinated Na^+ (1) near B. Usually, the peaks for higher-coordinated ions in simple glasses, such as silicate, borate, and phosphate glasses, are located in the upper-field of the NMR spectra [29]. Therefore, it is also reasonable to observe the peak for higher coordinated Na^+ in the upfield. However, for complex crystals or glasses that contain more than two network-forming oxides, it should be considered that the electron density of coordinated oxygen varies with respect to the neighboring element, such as Al^{3+} or B^{3+}. In this case, the chemical shift depends on the coordination number and the surrounding ions, such as Al^{3+} and B^{3+}. Considering these assumptions and the previous studies [15], the different chemical shifts for the Na^+ (1) and Na^+ (2) peaks were assumed to be affected by the coordination number and conjunctive Al^{3+} and B^{3+}. This implies that a larger chemical shift in the Na^+ spectrum corresponds to an increase in the coordination number or more Al surrounding Na^+. In light of these considerations, the

coordination number of Na^+ in each glass may have gradually increased following the increase in the number of Y^{3+}, and the elements surrounding Na^+ might have affected the change from B to Al. As shown in **Figure 1**, the addition of Y^{3+} ions produced higher coordinated Al species, and these Al species locally concentrated the oxygen ions. This concentrated oxygen result in an increase in the coordination number of Na^+. In addition, the ^{23}Na spectra of the La^{3+} glasses also shifted upfield as the La^{3+} content increased. This suggests that the above environmental change of Na^+ also occurred in the La^{3+}-containing glass. The difference of boron coordination is also considered to affect the oxygen concentration in the local structure and consequently the chemical shift of ^{23}Na NMR spectra of the glasses. However, as we discussed above, it was assumed that the amount of $^{[4]}B$ ratio was almost constant around 10%. Therefore, it is expected that the chemical shift of ^{23}Na NMR spectra was not affected by the boron coordination.

The relationship between the Al coordination state and physical properties in these glasses could be deduced because the fractions of $^{[5]}Al$ and $^{[6]}Al$ changed in response to the composition change, as shown above. In order to confirm this relationship, molar volume measurements were conducted, because the local structural change of Al coordination should directly affect spatial arrangement. The molar volumes steadily decreased in response to an increase in Y^{3+} content (**Figure 22**), which is caused by various effects. Firstly, rare-earth ions compensate negative charges of Al or B at a closer radius than Na^+, because they possess a much larger CFS than Na^+. Secondly, the production of higher-coordinated Al contributed to a decrease in molar volume because at higher coordination states of Al, atomic packing improves. This expectation can be clarified by comparing the molar volumes and fractions of various Al species in both Y^{3+}- and La^{3+}-containing glasses. When the compositions were (x, y) = (6, 0), (4.8, 0.4), and (3.96, 0.66), the summation of $^{[5]}Al$ and $^{[6]}Al$ and molar volume in Y^{3+}-containing glasses were not very different from those in La^{3+}-containing glasses (**Figure 22**, **Table 3**, and **Table 4**). However, when more rare-earth ions were present, as in the compositions (x, y) = (3, 1), (1.98, 1.32), (1.2, 1.6), and (0, 2), the summation of $^{[5]}Al$ and $^{[6]}Al$ in Y^{3+}-containing glasses became larger than that of La^{3+}-containing glass, while the molar volume of Y^{3+}-containing glasses became smaller. This comparison further proves that $^{[5]}Al$ and $^{[6]}Al$ lowered the molar volume of the glasses. According to Shannon [30], the ionic radius of Y^{3+} is 1.04 Å and that of La^{3+} 1.17 Å in 6-coordinated state. This difference may also affect the molar volume. However, there have been several reports concerning the relation between the molar volume and Al coordination [31] [32]. Therefore, Al coordination in this glass system must be one of the key-factor that affects the molar volume. In addition, it is expected that boron coordination number affect the molar volume. However, it was considered that boron coordination in our glass gave little influence on the molar volume, because the amount of $^{[4]}B$ in the samples were estimated to be almost constant as described.

Despite the above results, it remains challenging to elucidate the effects of $^{[5]}Al$ and $^{[6]}Al$ in oxide glass on certain physical properties, because other factors may

also affect the latter. Therefore, we plan to investigate the effects of $^{[5]}$Al and $^{[6]}$Al on physical and optical properties, including fictive temperature, the elastic modulus, refractive index, and photoluminescence, of the abovementioned glass system.

5. Conclusions

We here performed the structural analysis of yttrium sodium aluminoborate and lanthanum sodium aluminoborate glasses using magic angle spinning NMR. We elucidated that the addition of rare-earth ions (RE^{3+}) could result in higher-coordinated Al species ($^{[5]}$Al and $^{[6]}$Al), and that their amounts were proportional to the ratio of Y_2O_3 to Al_2O_3. Furthermore, the difference in cation field strength (CFS) between Y^{3+} and La^{3+} was confirmed to affect the generation of higher-coordinated Al. The CFS of rare-earth ions (Y^{3+} and La^{3+}) was sufficiently larger than that of Na^+ to make higher-coordinated Al without being affected by Na^+. It was also found that the coordination number of Na^+ in each glass gradually increased following the increase in the number of RE^{3+} ions. Further analysis such as ^{11}B MAS NMR or Soft X-ray spectroscopy for Na^+ can elucidate more detail about network structure or coordination environment, respectively.

In addition to the above results, it seems that the formation of $^{[5]}$Al and $^{[6]}$Al affected the physical properties (molar volume) due to better atomic packing with these higher-coordinated Al species. In order to clarify the relation between Al coordination number and physical properties in this glass system, further studies about fictive temperature or elastic module will be performed.

Although the unique affinity between RE^{3+} and Al in simple glasses has previously been reported, in this study, it was found that the same particular properties of RE^{3+} exist even in complex glasses. These results are expected to steadily lead to the development of ideal optical or building glass materials.

Acknowledgements

This study was carried out with the NMR spectrometer in the JURC at Institute for Chemical Research, Kyoto University. This work was supported by JSPS KAKENHI (grant number JP16K07640), Nippon Sheet Glass Foundation for Materials Science and Engineering, and Research Institute for Sustainable Humanosphere, Kyoto University.

References

[1] Sinton, C.W. and LaCourse, W.C. (2001) Experimental Survey of the Chemical Durability of Commercial Soda-Lime-Silicate Glasses. *Materials Research Bulletin*, **36**, 2471-2479. https://doi.org/10.1016/S0025-5408(01)00724-3

[2] El-Kheshen, A.A., Khaliafa, F.A., Saad, E.A. and Elwan, R.L. (2008) Effect of Al_2O_3 Addition on Bioactivity, Thermal and Mechanical Properties of Some Bioactive Glasses. *Ceramics International*, **34**, 1667-1673. https://doi.org/10.1016/j.ceramint.2007.05.016

[3] Stebbins, J.F., Kroeker, S., Lee, S.K. and Kiczenski, T.J. (2000) Quantification of Five- and Six-Coordinated Aluminum in Aluminosilicate and Fluoride-Containing

Glasses by High Field, High Resolution ^{27}Al-NMR. *Journal of Non-Crystalline Solids*, **275**, 1-6. https://doi.org/10.1016/s0022-3093(00)00270-2

[4] MacKenzie, K.J.D. and Smith, M.E. (2002) Multinuclear Solid State Nuclear Magnetic Resonance of Materials. Pergamon Press, Oxford.

[5] Stevensson, B. and Edén, M. (2013) Structural Rationalization of the Microhardness Trends of Rare-Earth Aluminosilicate Glasses: Interplay between the RE^{3+} Field-Strength and the Aluminum Coordinations. J. Non-Cryst. *Solids*, **378**, 163-167. https://doi.org/10.1016/j.jnoncrysol.2013.06.013

[6] Iftekhar, S., Pahari, B., Okhotnikov, K., Jaworski, A., Stevensson, B., Grins, J. and Edén, M. (2012) Properties and Structures of RE_2O_3-Al_2O_3-SiO_2 (RE=Y, Lu) Glasses Probed by Molecular Dynamics Simulations and Solid-State NMR: The Roles of Aluminum and Rare-Earth Ions for Dictating the Microhardness. *The Journal of Physical Chemistry C*, **116**, 18394-18406. https://doi.org/10.1021/jp302672b

[7] Rosales-Sosa, G.A., Masuno, A., Higo, Y., Inoue, H., Yanaba, Y., Mizoguchi, T., Umada, T., Okamura, K., Kato, K. and Watanabe, Y. (2015) High Elastic Moduli of a $54Al_2O_3$-$46Ta_2O_5$ Glass Fabricated via Containerless Processing. *Scientific Reports*, **5**, Article ID: 15233. https://doi.org/10.1038/srep15233

[8] Rosales-Sosa, G.A., Masuno, A., Higo, Y. and Inoue, H. (2016) Crack-Resistant Al_2O_3-SiO_2 Glasses. *Scientific Reports*, **6**, Article ID: 23620. https://doi.org/10.1038/srep23620

[9] Kelsey, K.E., Stebbins, J.F., Singer, D.M., Brown Jr., G.E., Mosenfelder, J.L. and Asimow, P.D. (2009) Cation Field Strength Effects on High Pressure Aluminosilicate Glass Structure: Multinuclear NMR and La XAFS Results. Geochim. *Geochimica et Cosmochimica Acta*, **73**, 3914-3933. https://doi.org/10.1016/j.gca.2009.03.040

[10] Morin, E.I., Wu, J. and Stebbins, J.F. (2014) Modifier Cation (Ba, Ca, La, Y) Field Strength Effects on Aluminum and Boron Coordination in Aluminoborosilicate Glasses: The Roles of Fictive Temperature and Boron Content. *Applied Physics A*, **116**, 479-490. https://doi.org/10.1007/s00339-014-8369-4

[11] Wu, J. and Stebbins, J.F. (2013) Temperature and Modifier Cation Field Strength Effects on Aluminoborosilicate Glass Network Structure. *Journal of Non-Crystalline Solids*, **362**, 73-81. https://doi.org/10.1016/j.jnoncrysol.2012.11.005

[12] Iftekhar, S., Grins, J., Gunawidjaja, P.N. and Edén, M. (2011) Glass Formation and Structure-Property-Composition Relations of the RE_2O_3-Al_2O_3-SiO_2 (RE = La, Y, Lu, Sc) Systems. *Journal of the American Ceramic Society*, **94**, 2429-2435. https://doi.org/10.1111/j.1551-2916.2011.04548.x

[13] Jaworski, A., Stevensson, B. and Edén, M. (2015) Direct ^{17}O NMR Experimental Evidence for Al–NBO Bonds in Si-Rich and Highly Polymerized Aluminosilicate Glasses. *Physical Chemistry Chemical Physics,* **17**, 18269-18272. https://doi.org/10.1039/C5CP02985F

[14] Chakraborty, I.N., Rutz, H.L. and Day, D.E. (1986) Glass Formation, Properties and Structure of Y_2O_3-Al_2O_3-B_2O_3 Glasses. *Journal of Non-Crystalline Solids*, **84**, 86-92. https://doi.org/10.1016/0022-3093(86)90764-7

[15] Brow, R.K., Tallant, D.R. and Turner, G.L. (1997) Polyhedral Arrangements in Lanthanum Aluminoborate Glasses. *Journal of the American Ceramic Society*, **80**, 1239-1244. https://doi.org/10.1111/j.1151-2916.1997.tb02970.x

[16] Rutz, H.L., Day, D.E. and Spencer, J.C.F. (1990) Properties of Yttria-Aluminoborate Glasses. *Journal of the American Ceramic Society*, **73**, 1788-1790. https://doi.org/10.1111/j.1151-2916.1990.tb09836.x

[17] Züchner, L., Chan, J.C.C., Müller-Warmuth, W. and Eckert, H. (1998) Short-Range Order and Site Connectivities in Sodium Aluminoborate Glasses: I. Quantification of Local Environments by High-Resolution ^{11}B, ^{23}Na, and ^{27}Al Solid-State NMR. *The Journal of Physical Chemistry B*, **102**, 4495-4506. https://doi.org/10.1021/jp980587s

[18] Du, L.S. and Stebbins, J.F. (2005) Site Connectivities in Sodium Aluminoborate Glasses: Multinuclear and Multiple Quantum NMR Results. *Solid State Nuclear Magnetic Resonance*, **27**, 37-49. https://doi.org/10.1016/j.ssnmr.2004.08.003

[19] Van, W.L., Züchner, L., Müller-Warmuth, W. and Eckert, H. (1996) $^{11}B^{27}\{Al\}$ and $^{27}Al^{11}\{B\}$ Double Resonance Experiments on a Glassy Sodium Aluminoborate. *Solid State Nuclear Magnetic Resonance*, **6**, 203-212. https://doi.org/10.1016/0926-2040(96)01228-3

[20] Chan, J.C.C., Bertmer, M. and Eckert, H. (1999) Site Connectivities in Amorphous Materials Studied by Double-Resonance NMR of Quadrupolar Nuclei: High-Resolution $^{11}B \leftrightarrow {}^{27}Al$ Spectroscopy of Aluminoborate Glasses. *Journal of the American Chemical Society*, **121**, 5238-5248. https://doi.org/10.1021/ja983385i

[21] Bertmer, M., Züchner, L., Chan, J.C.C. and Eckert, H. (2000) Short and Medium Range Order in Sodium Aluminoborate Glasses. 2. Site Connectivities and Cation Distributions Studied by Rotational Echo Double Resonance NMR Spectroscopy. *The Journal of Physical Chemistry B*, **104**, 6541-6553. https://doi.org/10.1021/jp9941918

[22] Morin, E.I. and Stebbins, J.F. (2016) Separating the Effects of Composition and Fictive Temperature on Al and B Coordination in Ca, La, Y Aluminosilicate, Aluminoborosilicate and Aluminoborate Glasses. *Journal of Non-Crystalline Solids*, **432**, 384-392. https://doi.org/10.1016/j.jnoncrysol.2015.10.035

[23] Deters, H., Camargo, A.S.S., Santos, C.N., Ferrari, C.R., Hernandes, A.C., Ibanez, A., Rinke, M.T. and Eckert, H. (2009) Structural Characterization of Rare-Earth Doped Yttrium Aluminoborate Laser Glasses Using Solid State NMR. *The Journal of Physical Chemistry C*, **113**, 16216-16225. https://doi.org/10.1021/jp9032904

[24] Deters, H., Lima, J.F., Magon, C.J., Camargo, A.S.S. and Eckert, H. (2011) Structural Models for Yttrium Aluminium Borate Laser Glasses: NMR and EPR Studies of the System $(Y_2O_3)_{0.2}$-$(Al_2O_3)_x$-$(B_2O_3)_{0.8-x}$. *Physical Chemistry Chemical Physics*, **13**, 16071-16083. https://doi.org/10.1039/c1cp21404g

[25] He, M., Chen, X.L., Zhou, T., Hu, B.Q., Xu, Y.P. and Xu, T. (2001) Crystal Structure and Infrared Spectra of $Na_2Al_2B_2O_7$. *Journal of Alloys and Compounds*, **327**, 210-214. https://doi.org/10.1016/S0925-8388(01)01561-4

[26] Perras, F.A. and Bryce, D.L. (2012) Multinuclear Magnetic Resonance Crystallographic Structure Refinement and Cross-Validation Using Experimental and Computed Electric Field Gradients: Application to $Na_2Al_2B_2O_7$. *Journal of Physical Chemistry C*, **116**, 19472-19482. https://doi.org/10.1021/jp308273h

[27] Gresch, R. and Müller-Warmuth, W. (1976) ^{11}B and ^{27}Al NMR Studies of Glasses in the System Na_2O-B_2O_3-Al_2O_3 ("NABAL"). *Journal of Non-Crystalline Solids*, **21**, 31-40. https://doi.org/10.1016/0022-3093(76)90088-0

[28] Chakraborty, I.N. and Day, D.E. (1985) Effect of R^{3+} Ions on the Structure and Properties of Lanthanum Borate Glasses. *Journal of the American Ceramic Society*, **68**, 641-645. https://doi.org/10.1111/j.1151-2916.1985.tb10117.x

[29] Stebbins, J.F. (1998) Cation Sites in Mixed-Alkali Oxide Glasses: Correlations of NMR Chemical Shift Data with Site Size and Bond Distance. *Solid State Ionics*, **112**, 137-141. https://doi.org/10.1016/S0167-2738(98)00224-0

[30] Shannon, R.D. (1969) Revised Effective Ionic Radii and Systematic Studies of Interatomic Distances in Halides and Chalcogenides. *Acta Crystallographica Section A*, **32**, 751-767. https://doi.org/10.1107/S0567739476001551

[31] Allwardt, J.R., Stebbins, J.F., Schmidt, B.C., Frost, D.J., Withers, A.C. and Hirschmann, M.M. (2005) Aluminum Coordination and the Densification of High-Pressure Aluminosilicate Glasses. *American Mineralogist*, **90**, 1218-1222. https://doi.org/10.2138/am.2005.1836

[32] Kelsey, K.E., Stebbins, J.F., Mosenfelder, J.L. and Asimow, P.D. (2009) Simultaneous Aluminum, Silicon, and Sodium Coordination Changes in 6 GPa Sodium Aluminosilicate Glasses. *American Mineralogist*, **94**, 1205-1215. https://doi.org/10.2138/am.2009.3177